JOURNAL OF CATALYSIS **180,** 24–35 (1998)
ARTICLE NO. CA982257

Catalytic Solid State Reactions on the Surface of Nanoscale Metal Oxide Particles

Yan Jiang, Shawn Decker, Cathy Mohs, and Kenneth J. Klabunde

Department of Chemistry, Kansas State University, Manhattan, Kansas 66506

Received December 18, 1997; revised August 14, 1998; accepted August 17, 1998

Core–shell nanoparticles of metal oxides ([Fe_2O_3]MgO, [Fe_2O_3]CaO, [V_2O_3]MgO, and the other first-row transition metal shell materials coated on nanoparticles of MgO or CaO) have been studied as destructive adsorbents for CCl_4, $CHCl{=}CCl_2$, $C_6H_4Cl_2$, $CH_3P(O)(OCH_3)_2$, and SO_2. A catalytic effect due to the transition metal shell material has been observed, where solid state ion–ion exchange takes place, thus allowing penetration into the MgO or CaO particles and thereby regenerating the transition metal oxide for additional catalytic action. Due to this catalytic effect, the destructive adsorption reaction became nearly stoichiometric, and therefore much higher capacities for destruction/immobilization of the adsorbate under study were realized. For example, the reaction $CCl_4 + [V_2O_5]MgO \rightarrow CO_2 + [V_2O_5]MgCl_2$ is greatly enhanced by the presence of the V_2O_5, and VCl_5 or VCl_3 appear to be intermediates in the process. The catalytic effects are proposed to be due to the intermediacy of transition metal chlorides, phosphates, or sulfites, which are mobile and seek out reactive sites on the MgO or CaO nanoparticles where ion–ion exchange can most readily take place, thereby regenerating the transition metal oxide catalyst.

INTRODUCTION

Unusual, if not remarkable, catalytic effects have recently been reported, where a monolayer of Fe_2O_3 on MgO (or CaO) led to greatly enhanced efficiencies for chlorocarbon destruction and sulfur dioxide adsorption (1–3):

$$2[Fe_2O_3]MgO + CCl_4 \xrightarrow{400^\circ C} 2[Fe_2O_3]MgCl_2 + CO_2 \quad [1]$$

$$2[Fe_2O_3]CaO + 2SO_2 \xrightarrow{425^\circ C} [Fe_2O_3]CaSO_4 + CaS. \quad [2]$$

In the chlorocarbon case (reaction [1]) the presence of the iron oxide catalytically enhanced solid state ion–ion exchange deep into the MgO(CaO) particle, and the formation of $MgCl_2$($CaCl_2$) on the surface did not serve to protect the inner core (as is the case in the absence of the Fe_2O_3).

In general terms, these results have been interpreted in terms of reaction steps that are all thermodynamically favorable, as is shown in Fig. 1; in the reaction of CCl_4 with [Fe_2O_3]CaO, $FeCl_3$ is proposed to form first, followed by [$FeCl_3$]-CaO $\rightarrow$ [Fe_2O_3]$CaCl_2$ (i.e., O^{2-}–Cl^- exchange). A second approach of CCl_4 causes $FeCl_3$ to form again, and (it is proposed that) this mobile phase seeks out more CaO, perhaps at fissures or edges/corners of the CaO nanocrystal. Repetition of these steps can lead to complete consumption of the core of CaO to form $CaCl_2$, such that this solid–gas reaction becomes stoichiometric. This is truly a catalytic effect of Fe_2O_3, since it has been shown that even after extensive CCl_4 reaction (but less than stoichiometric), Fe_2O_3 is present, having been efficiently regenerated by the remaining core oxide (4).

Herein is reported further work dealing with solid–gas reactions showing that this catalytic chemistry is rather general. All the first-row transition metal oxides have been examined, and several destructive adsorption processes with chlorocarbons, organophosphorus compounds, and acid gases have been investigated.

EXPERIMENTAL

Preparation of Samples

CP-MgO and CP-CaO

Conventional samples were prepared by heating commercially available CM-MgO (10–30 m^2/g; designated CM-) or CM-CaO (1–3 m^2/g) in water at 80°C overnight under argon. After filtration the filter cake was dried in an oven at 120°C for 2 h, broken into small pieces, and then heated under vacuum at 120°C overnight. The resulting CP-Mg$(OH)_2$ or CP-Ca$(OH)_2$ was stored under argon until needed. Samples of CP-MgO (CP-CaO) were prepared by heating portions of the hydroxides to 500°C under dynamic vacuum and held at temperatures overnight. Surface areas ranged from 130 to 250 m^2/g for CP-MgO and 50 to 100 m^2/g for CP-CaO.

AP-MgO and AP-CaO

The aerogel/hypercritical drying procedure (samples designated AP-) has been described earlier (3). Figure 2 summarizes the steps involved. Surface areas obtained ranged from 250 to 500 m^2/g for AP-MgO and 120 to 160 m^2/g for AP-CaO.

0021-9517/98 $25.00

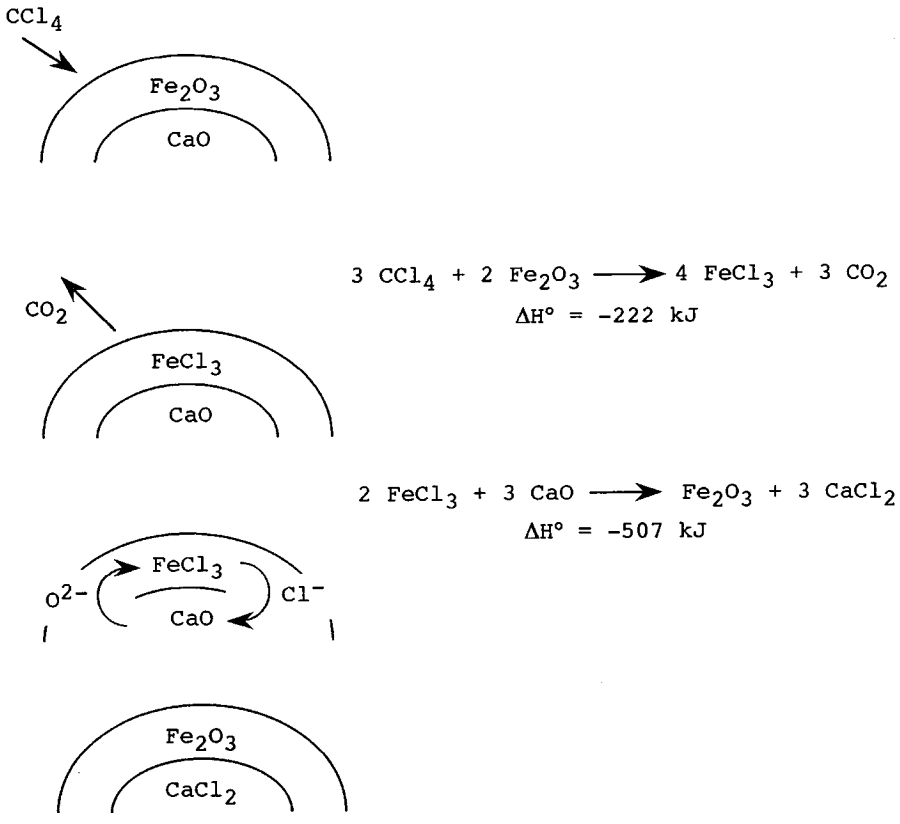

FIG. 1. Reaction steps on core-shell Fe_2O_3-coated nanoparticles of CaO with gaseous CCl_4.

Transition Metal Oxide-Coated MgO and CaO

Metal acac procedure. Metal acetylacetonates (acac) were dissolved in THF and allowed to adsorb onto MgO and CaO samples as described earlier for iron oxide on MgO (1, 3).

Metal nitrate procedure. A desired amount of $Fe(NO_3)_3 \cdot 9H_2O$ was placed in a round-bottom flask equipped with a thermometer and magnetic stir bar, and 30 ml of doubly distilled water was added with stirring for 5 min. Then 1.0 g of CP-MgO (or AP-MgO) was added and the flask was sealed and stirred for 48 h. Two methods were used to remove the water: (1) evaporation, in which all the iron nitrate was forced to deposit on the MgO surface; and (2) filtration and then rinsing with water, during which impregnation of the MgO occurred in the 48-h stirring period.

The samples were dried at 200°C in an oven and stored in vials under argon in the dark.

Samples prepared in this way led to wt% loadings of Fe of 1, 2, 3, 13, 23, 38, 61, and 77%, where the amount of $Fe(NO_3)_3 \cdot 9H_2O$ used was 0.072, 0.145, 0.217, 1.09, 2.17, 2.17, 4.41, 11.43, and 24.09 g, respectively. The samples ranged in color from light tan to dark red, and before use were heat treated at 500°C under a flow of oxygen for 3 h.

Characterization of Samples

Methods for obtaining surface areas, X-ray diffraction (XRD) data, and other procedures have been briefly described earlier (3) and in detail (5). Elemental analyses were performed by Galbraith Laboratories or Desert Analytics.

Destructive Adsorption by the U-Tube Pulsed Reactor GC Method

This procedure has been described earlier (3, 5, 6). Quartz reactor tubes were used with 0.1 g of destructive adsorbent. For these experiments, the total amount of material decomposed was calculated from GC peak areas calibrated with standard injections; for example,

$$\%CCl_4 \text{ decomposed} = \frac{V_{(\mu L)}\ CCl_4 \text{ injected} - V_{(\mu L)} \text{ eluted}}{V_{(\mu L)} CCl_4 \text{ injected}}.$$

Experimental Conditions

Columns Used

CCl_4 studies. A Gow Mac Series 580 gas chromatograph was used with a 18 ft × 1/8 inch (i.d. = 0.085) stainless steel 80/100 mesh Chromosorb W-HP column with 10% SE-30 stationary phase, column temperature of 70, 85, or

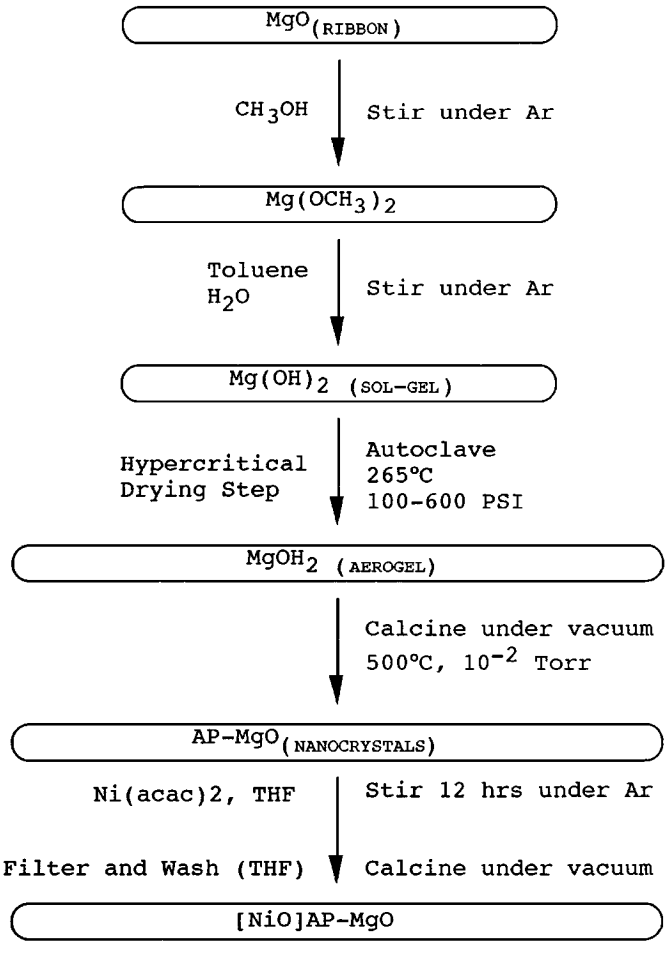

FIG. 2. Flow chart for the preparation of AP-MgO and [NiO]AP-MgO.

100°, injector 120°, detector 140°, and a flow rate of 30 ml/min of He.

DMMP studies. A 6 ft × $\frac{1}{4}$ inch glass 4% Carbowax 2.0M on Carbograph 1 was used, 80/100 mesh with a column temperature of 200°C, injector 225°C, detector 210°C, and a flow rate of 30 ml/min of He.

$CHCl{=}CCl_2$ studies. An 18 ft × 1/8 inch o.d., 0.085 i.d., 80/100 chromosorb W-HP was used with SE30 stationary phase, column temperature of 85°C, injector 120°C, detector 140°C, and a flow rate of 30 ml/min of He.

$C_6H_4Cl_2$ studies. A 7 ft × 1/8 inch o.d., 0.085 i.d., 60/80 Poropak S was used, column temperature of 125°C, injector 220°C, detector 140°C, and a flow rate of 30 ml/min of He.

X-Ray Photoelectron Spectroscopy

Measurements were made on an AEI (Kratos) ES200 X-ray photoelectron spectrometer using Mg$K\alpha$ X-radiation at a base pressure of 10^{-8} to 10^{-10} Torr. All spectra, including core level and valence band, were recorded at a fixed retardation ratio (FRR) mode with a ratio of 1:23. The binding energy of the most intense peak of the carbon 1*s* region was set as 284.6 eV for calibration purposes.

Samples were stored under argon in sealed glass vials. The powder was spread evenly and pressed firmly on a double-sided adhesive tape with one side adhering to the copper sample probe (the powder completely covered the tape). The sample was immediately inserted into the XPS chamber.

Data analysis and curve fitting were carried out as described earlier. The Gaussian/Lorentzian mix ratio was taken as 0.5 for all component peaks (7, 8).

Elemental compositions were obtained from intensities of the photoelectron peaks corrected for density of the sample and the inelastic mean free path (5). Photoelectron cross sections used in the calculations were adopted from Scofield's values (9) (Mg 2*p*, 0.3604; Fe2*p*, 15.97; Mn2*p*, 13.62; V2*p*, 9.59; Ni2*p*, 21.10; and Cl2*p*, 2.36).

Atomic Force Microscopy

Samples of NiO, Fe_2O_3, V_2O_5, and MnO_2 on AP-MgO were studied. Imaging of the sample surfaces was carried out using a SPM 30 from Wyco, Inc. (Tucson, AZ) in the contact mode. A 100-μm-long rectangular tip was used. The force intensity was about 8 to 15 × 10^{-8} N and the sample surfaces were scanned using the height mode, where the force and hence the distance between the tip and the surface were kept constant. All images (256 × 256 pixels) were obtained in air at room temperature. Different parts of the surface of each sample were studied to be certain that the observed structure was representative of the whole.

RESULTS

Carbon Tetrachloride Destructive Adsorption on Core–Shell Nanocrystals of [M_xO_y]MgO, where *M* = Sc, Ti, V, Cr, Mn, Fe, Co, Ni, Cu, Zn

Objectives and Synthesis of Samples

The objective of the following experiments was to determine if the catalytic ability for CCl_4 destructive adsorption varied with the change in transition metal oxide as the shell material. Therefore, a series of core–shell [M_xO_y]MgO particles was prepared by treating small crystals of MgO with $M(acac)_z$ in THF or other appropriate solvent. The MgO was pretreated to 500°C under vacuum, cooled to room temperature, and allowed to contact the $M(acac)_3$ solution at room temperature under argon. After standing, the $M(acac)_2$ was partially adsorbed onto the surface of the MgO.

Further heat treatment led to production of the core–shell particles.

TABLE 1

Physical Properties, Elemental Analyses, and XPS Data on [M_xO_y]AP-MgO Samples Prepared

	Color	Surface area (m^2/g)	Crystallite size (nm)	M%[a]	Mg%[a]	M/Mg ratio[b]	M/Mg ratio[c]	Oxidation state of M[c]
[Sc_2O_3]MgO	White	92	9.5	3.59	47.4	0.076		
[TiO_2]MgO	Yellow	240	5.0	5.48	42.4	0.129		
[V_2O_5]MgO	Dark green	230	5.0	2.99	42.4	0.071	0.0124	+5
[Cr_2O_3]MgO	Purple	240	4.4	0.094	42.9	0.002		
[MnO_2]MgO	Brown	290	4.7	4.54	41.1	0.111	0.0753	+4
[Fe_2O_3]MgO	Orange	290	4.4	2.51	50.0	0.050	0.326	+3[f]
[CoO]MgO	Gray	240	4.9	3.42	39.2	0.087		
[NiO]MgO	Light green	250	4.3	3.59	49.3	0.073	0.423	+2
[CuO]MgO	Light blue	240	6.7	6.72[d]	39.7	0.169		
[ZnO]MgO	White	240	4.4	6.62[d]	49.4	0.134		
AP-MgO[e]	White	400	4.3	—		—		

[a] By mass.
[b] For bulk sample.
[c] By XPS.
[d] Cu and Zn-acac complexes were not highly soluble in THF and some undissolved Cu(acac) and $Zn(acac)_2$ may have remained after filtration.
[e] All samples were prepared from Ap-MgO.
[f] SQUID magnetometry data strongly suggest Fe^{3+}.

Two types of well-characterized MgO powders were used: nanocrystals labeled AP-MgO (for aerogel prepared) and microcrystals, labeled CP-MgO (for conventionally prepared).

Characterization of [M_xO_y]MgO Samples before CCl_4 Reaction

Table 1 summarizes physical properties and elemental analyses for all [M_xO_y]AP-MgO samples prepared, as well as XPS data for selected samples. Figure 3 shows complete XPS spectra for a [NiO]AP-MgO sample, and Figs. 4 and 5 show Mg2*p*, Mn2p, and V2p core level spectra. From these data oxidation states could be determined for the transition metal M ions (before CCl_4 reactions) and ratios of M/Mg on the surface. From Table 1 it should be noted that for V and Mn the surface ratios were not that different from the bulk ratio, whereas for Fe and Ni the surface ratios were much higher, indicating that the Fe_2O_3 and NiO resided mainly at the surface, whereas for V and Mn during the heat treatment step (500°C) apparently V and Mn ions were able to permeate the MgO nanocrystal. However, XRD spectra for these samples only showed the pattern for MgO, and no evidence for crystallites of transition metal oxide was ever seen. However, for the [CuO]AP-MgO sample some Cu metal was observed along with MgO.

Reactions with CCl_4

Large aliquots of CCl_4 with short times between pulses (first stage). A quartz U-tube reactor attached to a gas chromatograph was employed (Fig. 6). A 0.1-g sample of [M_xO_y]MgO was placed in the U-tube, and at the desired temperature under He flow, 4 μl CCl_4 was injected, and gaseous products were analyzed by GC. Injections were at 3-min intervals until 160 μl had been injected (the theoretical maximum was 120 μl for a stoichiometric reaction $2MgO + CCl_4 \rightarrow 2MgCl_2 + CO_2$). This procedure was utilized as a method of rapidly gaining comparative data on all of the samples.

The major gaseous product was CO_2 and the amount eluted decreased with increasing injection number. When CCl_4 began to break through the bed, this injection was noted as the breakthrough number. In some cases C_2Cl_4 was also detected as a trace product, and the amount eluted with each injection was fairly constant.

Table 2 summarizes results of these rapid comparison studies.

Smaller aliquots of CCl_4 with larger times between pulses (second stage). After determination of which [M_xO_y]MgO samples were most promising for CCl_4 destructive adsorption, more demanding experiments were devised so that more quantitative information would be accessible. In these experiments 0.10 g of [M_xO_y]MgO was used with 1-μl injections of CCl_4 and 6-min intervals. This procedure allowed more time for Cl^-/O^{2-} solid state exchange to take place in an attempt to maximize efficiency.

Figure 7 illustrates the results of these second stage studies and clearly shows that the iron, manganese, and especially vanadium are superior to the others. This remarkable result with [V_xO_y]MgO was repeated with the same sample and with another sample made from completely new starting materials, and reproducibility was very good (Table 3).

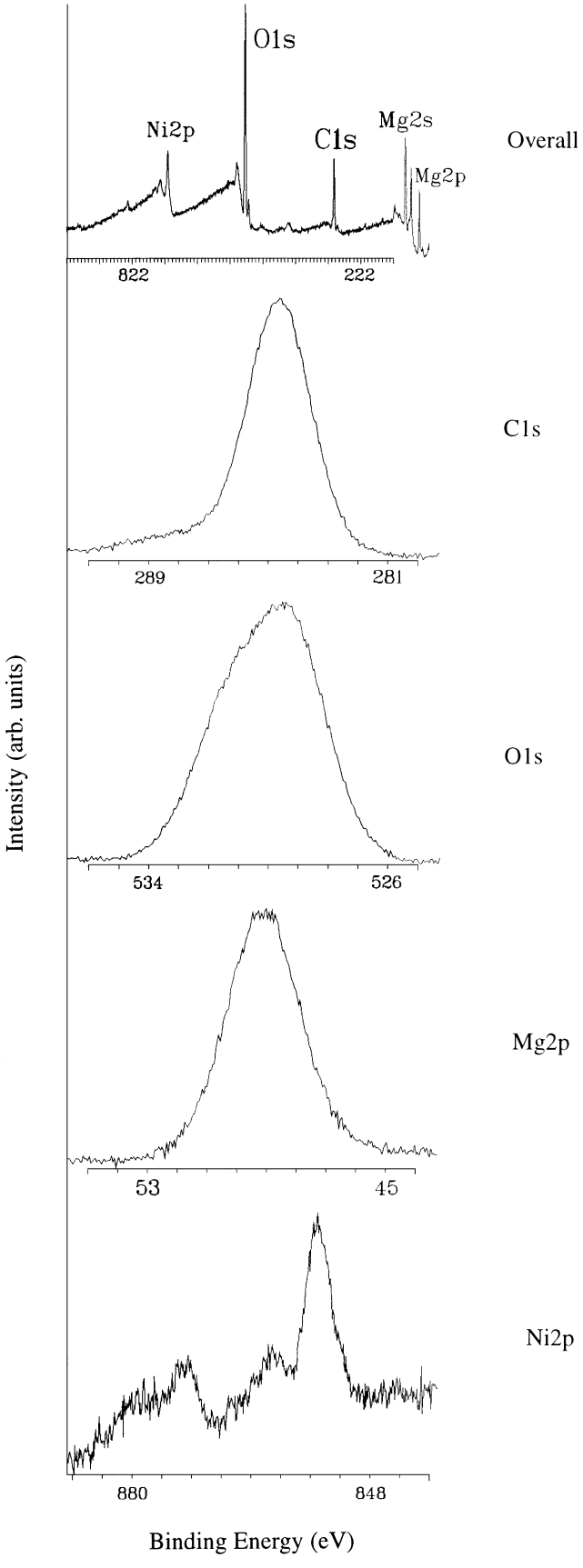

FIG. 3. XPS spectrum for [NiO]AP-MgO.

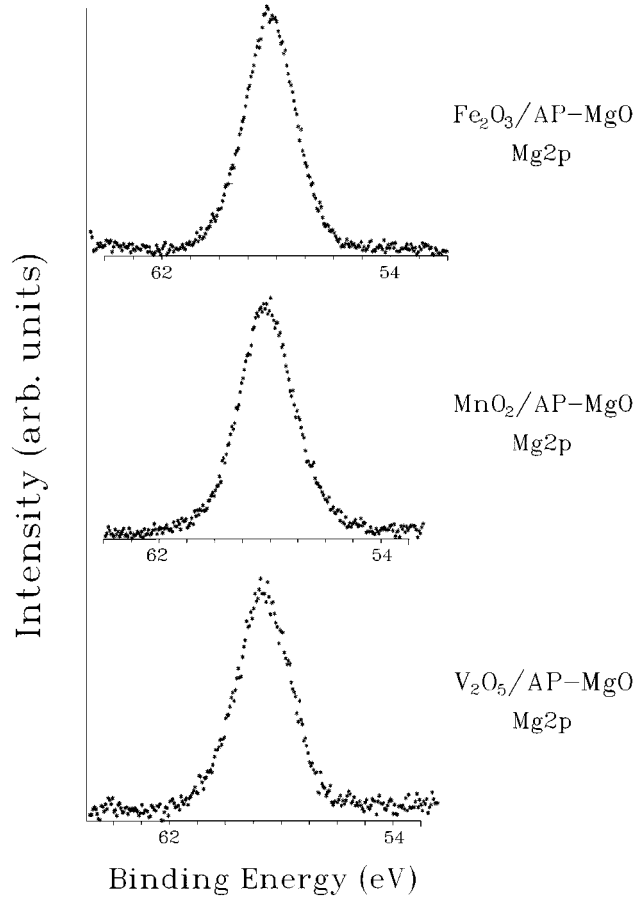

FIG. 4. Mg_{2p} core level XPS spectra of three metal oxide-coated AP-MgO samples.

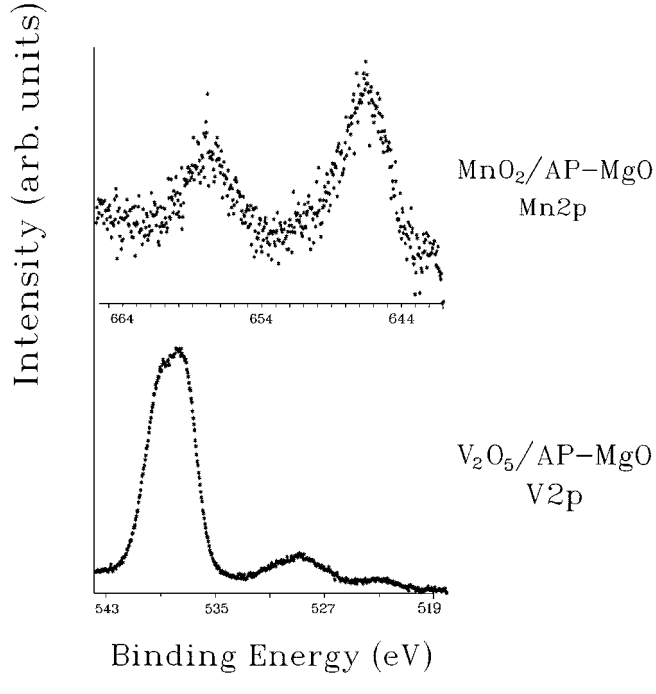

FIG. 5. Core level XPS spectra of metal oxide-coated AP-MgO samples.

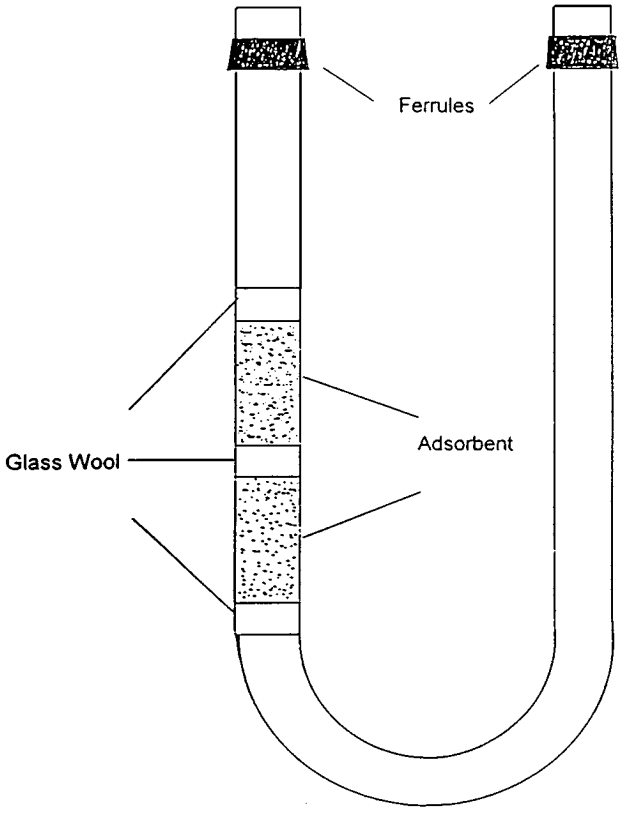

FIG. 6. Packing of quartz reaction tube.

Characterization of Solid Residues after Reaction with CCl_4

After reaction the solid residues were usually black and exhibited much lower surface areas, usually 20–50 m^2/g. Powder XRD of samples after CCl_4 reaction showed strong patterns for $MgCl_2$ and $MgCl_2 \cdot H_2O$ with weak signals for residual MgO (except for the Sc_xO_y-coated and Cr_xO_y-coated samples, for which less efficient conversion took place and weaker $MgCl_2$ signals were found). For example, $[Mn_xO_y]$MgO reacted almost completely (Fig. 8), whereas uncoated MgO after reaction showed very weak $MgCl_2$ signals with MgO signals remaining very strong. These results demonstrate clearly that most of the transition metal oxide coatings were very effective in promoting Cl^-/O^{2-} exchange so that nearly all of the MgO was converted to $MgCl_2$. It seems conclusive that when only nanocrystalline MgO is present, only the surface reacts with CCl_4, but in the presence of a small amount of M_xO_y nearly stoichiometric reactions take place.

Morphological changes on the surface of the samples were followed by atomic force microscopy. When efficient reactions were encountered, striking changes in morphology occurred (as might be expected from the severe degrading of surface area). An example is shown in Fig. 9, where [NiO]MgO before reaction and after reaction (50 μl CCl_4) is shown. The small particles before reaction quickly converted to much larger, layered particles of $NiCl_2$–$MgCl_2$.

Conclusions

The presence of a small amount of M_xO_y (except Sc_xO_y) greatly enhanced the capacity for destructive adsorption of CCl_4. The effectiveness for promoting this reaction followed the order V > Mn > Co > Fe > Zn > Ti > Cu > Ni > Cr > none > Sc.

This conclusion was supported by quantitative determinations of CO_2 formed, CCl_4 destroyed, and XRD of solids.

The $[V_2O_5]$MgO sample was superior and results were highly reproducible. In experiments in which 90% of the theoretical maximum of CCl_4 was passed over the $[V_2O_5]$MgO sample, 90% was destroyed, or in other words 0.4 mol CCl_4 destroyed/mol MgO (theoretical maximum is 0.5).

1,3-Dichlorobenzene and Trichloroethene Destructive Adsorption on $[M_xO_y]$MgO, where M = V, Fe

Two of the best destructive adsorbents $[V_2O_5]$AP-MgO and $[Fe_2O_3]$AP-MgO were studied with two especially recalcitrant organochlorine compounds. The compounds chosen were 1,3-dichlorobenzene (DCB), a hazardous product from combustion of treated wood and plastics (10–12), and trichloroethene (TCE), a widely used dry cleaning solvent.

In the case of DCB, benzene, carbon monoxide, and water were detected as volatile products during the U-tube pulsed reaction experiments. Graphite also seemed to be a product since the adsorbents quickly became very dark in color. A likely reaction stoichiometry is (reaction temperature = 425°C)

TABLE 2

Results of Destructive Adsorption of CCl_4 on 10 Transition Metal Oxide-Coated MgO and Pure MgO Adsorbents

Samples	% of CCl_4 decomposed (ratio of mol/mol)[a]	Breakthrough numbers	Final peak area ratio of CO_2/CCl_4
AP-MgO	13 (0.09)	0	1.0×10^{-2}
$[Sc_2O_3]$AP-MgO	5 (0.03)	0	3.3×10^{-2}
$[TiO_2]$AP-MgO	40 (0.27)	3	6.1×10^{-2}
$[V_2O_5]$AP-MgO	59 (0.39)	16	1.6×10^{-2}
$[Cr_2O_3]$AP-MgO	14 (0.09)	0	1.9×10^{-2}
$[MnO_2]$AP-MgO	52 (0.34)	13	3.4×10^{-2}
$[Fe_2O_3]$AP-MgO	44 (0.29)	8	8.4×10^{-2}
[CoO]AP-MgO	49 (0.32)	8	5.6×10^{-2}
[Nio]AP-MgO	28 (0.19)	4	8.4×10^{-2}
[CuO]AP-MgO	36 (0.24)	5	7.9×10^{-2}
[ZnO]AP-MgO	42 (0.28)	5	4.0×10^{-2}

[a] Moles of CCl_4 decomposed per mole of MgO present × 100.

TABLE 3

Reproducibility of CCl_4 Destruction on Different [V_xO_y]MgO Samples (1-μl Injections of CCl_4 for Each Experiment with 6-min Intervals between Injections)

	%CCl_4 destroyed	Mol CCl_4 destroyed/mol MgO[b]	Breakthrough numbers	Final ratio of CO_2/CCl_4 (peak areas)	Number of injections
Sample 1	87	0.32	70	0.02	100
Sample 2[a]	90	0.40	84	0.02	107

[a] Prepared from new starting materials.

[b] Assuming $2MgO + CCl_4 \rightarrow 2MgCl_2 + CO_2$ balanced equation (ignoring the small amount of V_2O_5 present). Therefore the maximum ratio to be expected would be 0.50 for a stoichiometric reaction.

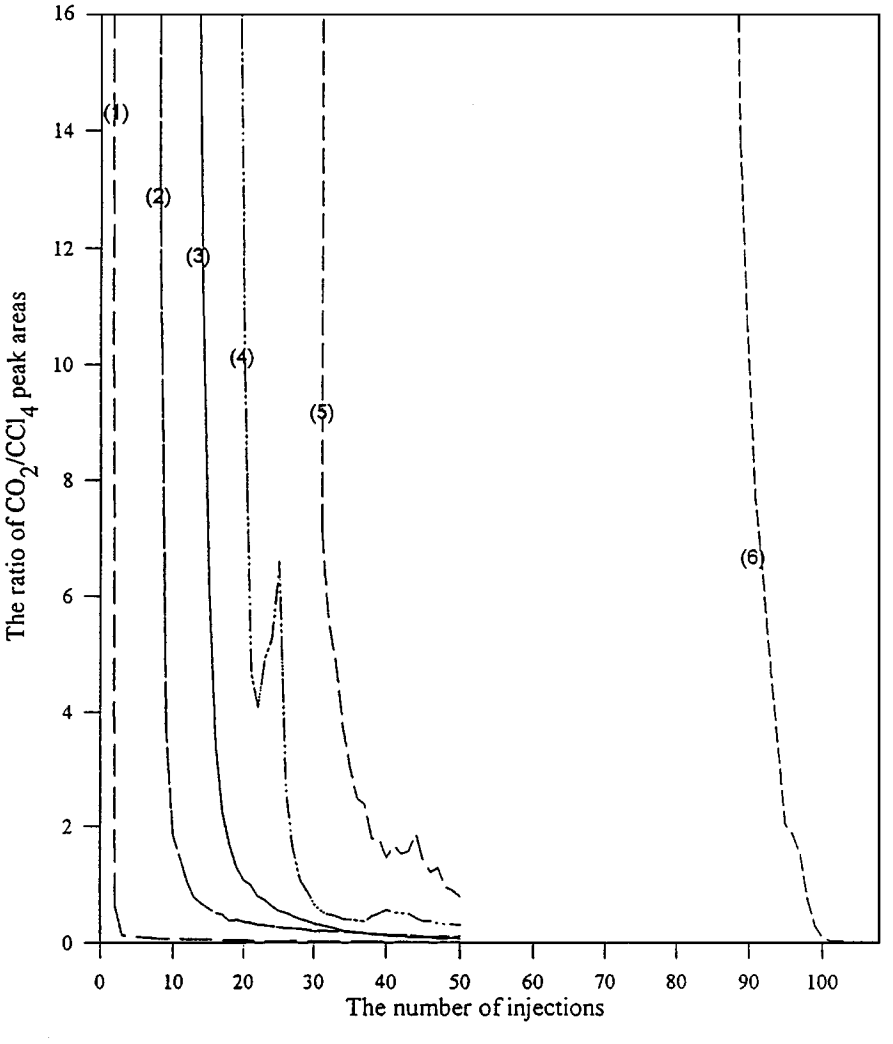

FIG. 7. Comparisons of CCl_4 reaction efficiencies on five destructive adsorbents showing the best performance and compared with pure AP-MgO.

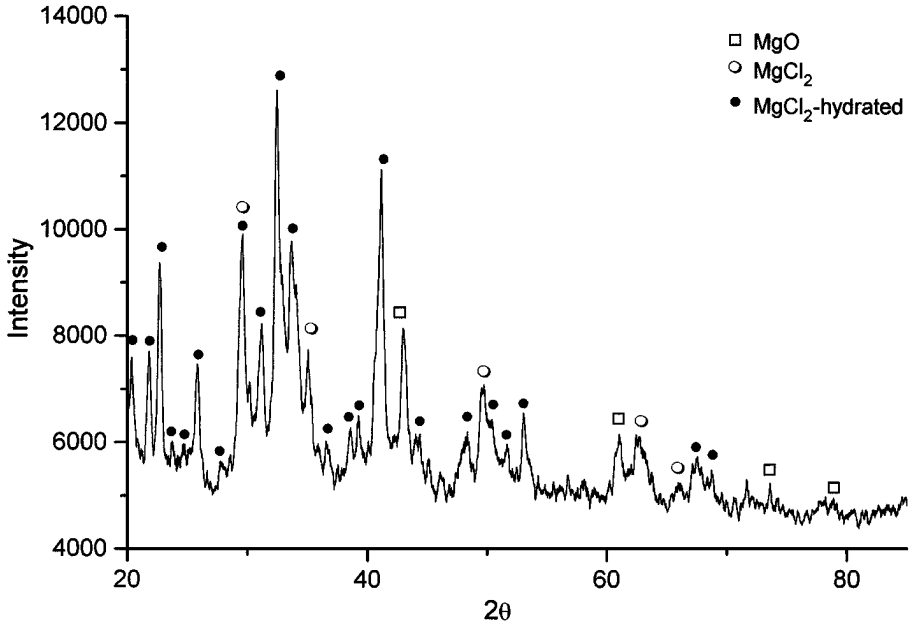

FIG. 8. The XRD spectrum of $[Mn_xO_y]$AP-MgO/CCl_4 as an example of peak patterns.

$$2C_6H_4Cl_2 + 2MgO \rightarrow C_6H_6 + 2MgCl_2 + CO + 5C + H_2O. \quad [3]$$

Table 4 summarizes some of the data collected. A direct comparison with AP-MgO clearly showed that the presence of V_2O_5 or Fe_2O_3 was quite beneficial. Indeed, after breakthrough DCB continued to be partially destructively adsorbed even out to over 200 μl, showing that the reaction could be driven essentially to completion, if a 1 : 1 stoichiometric ratio of DCB : MgO is assumed.

Since the experiments were very long, AP-MgO and $[Fe_2O_3]$AP-MgO were not carried out to 255 μl as was the $[V_2O_5]$AP-MgO sample. However, it is clear that Fe_2O_3 and especially V_2O_5 have a dramatic effect on improving efficiency in this DCB chemistry.

Interestingly, this beneficial catalytic effect of V_2O_5 and Fe_2O_3 was not observed with trichloroethene (TCE). With TCE, which yielded CO, CO_2, and H_2O as volatile products, and $MgCl_2$ and C as solids, the reaction may proceed as shown in Eqs. [4] and [5]:

$$2C_2HCl_3 + 3MgO \rightarrow CO_2 + H_2O + 3MgCl_2 + 3C \quad [4]$$

or

$$\rightarrow 2CO + H_2O + 3MgCl_2 + 2C. \quad [5]$$

In the TCE system the effectiveness for destructive adsorption was in the order AP-CaO > AP-MgO > $[Fe_2O_3]$AP-MgO > $[V_2O_5]$AP-MgO, with breakthrough numbers ranging only from 1 to 3, and percentage TCE destroyed after 32 μl was injected of 28% for (AP-MgO), 16% for $[Fe_2O_3]$AP-MgO, and 10% for $[V_2O_5]$AP-MgO.

Obviously, the catalytic effect of transition metal oxides depends a great deal on the intimate mechanistic details that are, of course, different for each different chlorocarbon under study. Since carbon deposition is a likely mode of reactive site poisoning, it is interesting that $C_6H_4Cl_2$ conversion is not so affected. This suggests that the problem with C_2HCl_3 lies with the fine mechanistic details of the carbon deposition step, or it may be that the initial C_2HCl_3–transition metal oxide interaction is not favorable or is very slow. More information is needed before further discussion is warranted.

TABLE 4

Destructive Adsorption of Dichlorobenzene on Selected Samples

	AP-MgO	$[V_2O_5]$MgO	$[Fe_2O_3]$MgO
Number of injections	50	255	132
Breakthrough	4	208	130
% DCB destroyed	62% of 50 μL	90% of 255 μL or 0.8 mol DCB/mol MgO	100% of 130 μL

Dimethylmethylphosphonate Destructive Adsorption on $[M_xO_y]$AP-MgO, where M = Fe

In earlier work it was reported that DMMP (13) was destructively adsorbed on high surface MgO, and about two surface MgO moieties were required to destroy one DMMP molecule (6, 14). Equation [6] shows the surface chemistry that takes place (14):

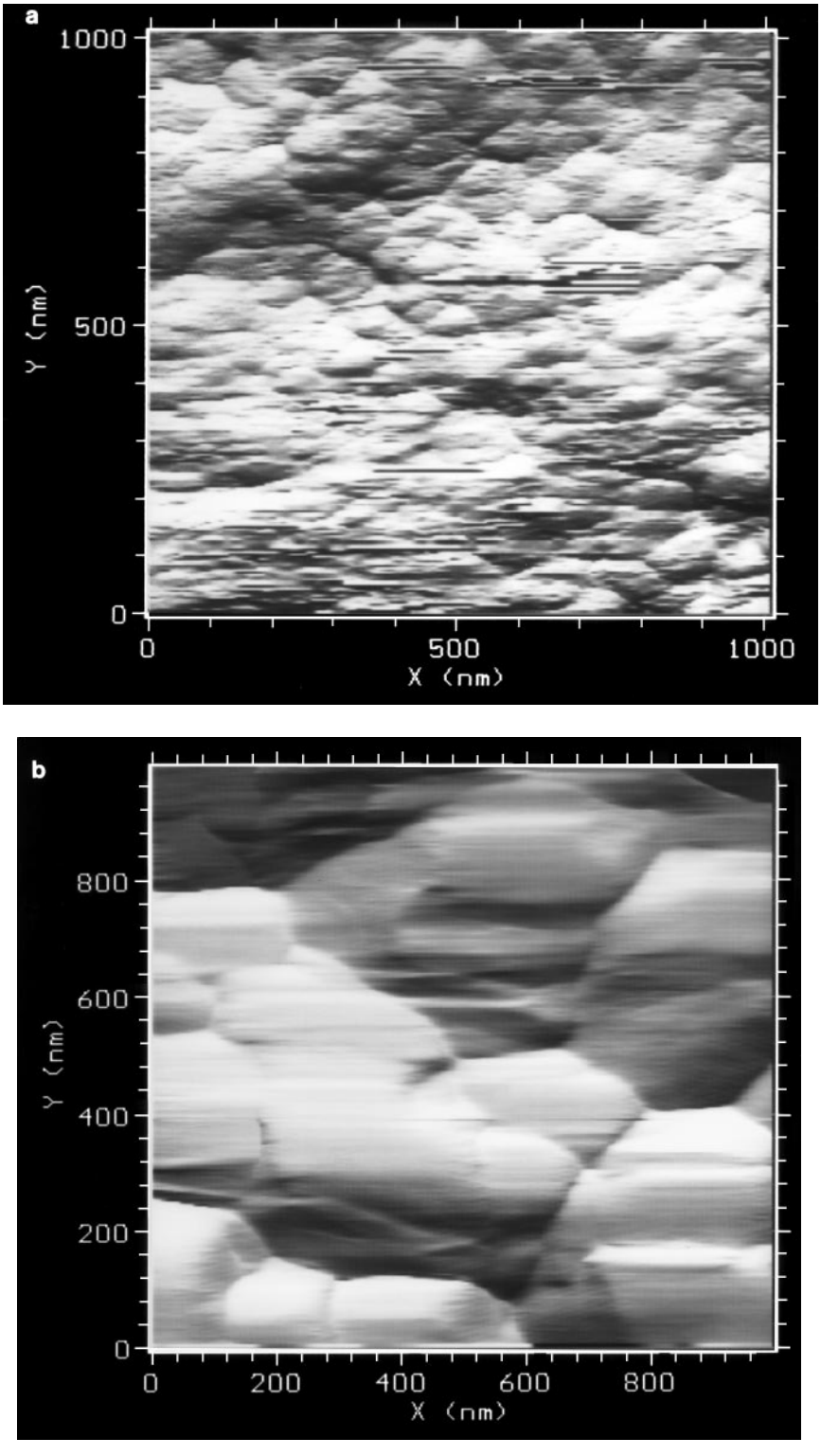

FIG. 9. (a) AFM image (1000 nm^2) of [NiO]AP-MgO sample surface. (b) AFM image (1000 nm^2) of [NiO]AP-MgO sample surface after reaction with CCl_4.

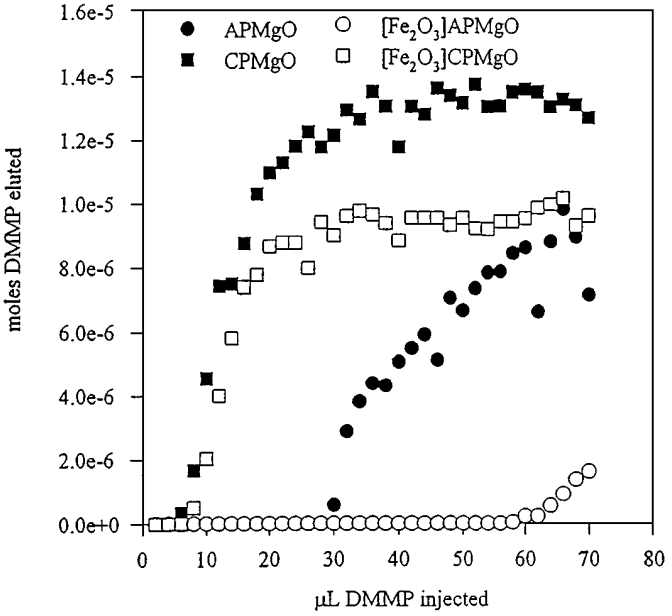

FIG. 10. Destructive adsorption of DMMP with AP-MgO, $[Fe_2O_3]$AP-MgO, CP-MgO, and $[Fe_2O_3]$CP-MgO, where 2 μL of DMMP was injected every 6 min.

$$\underset{\text{DMMP}}{CH_3O\text{-}P(=O)(OCH_3)\text{-}CH_3} \xrightarrow{MgO_{(s)}} [CH_3O\text{-}P\text{-}CH_3]_{ads} \longrightarrow HOCH(=O) + CH_3OH + H_2O \quad [6]$$

Since this chemistry was surface limited, the higher surface area MgO samples exhibited more capacity for DMMP destruction, as expected.

Based on the success achieved with enhancement of chlorocarbon decomposition on $[M_xO_y]$AP-MgO, we also looked at DMMP with $[Fe_2O_3]$MgO samples.

Using the U-tube reactor GC system, a study was carried out to determine the optimum temperature, 300, 400, or 500°C, and it was found that 500°C was best. Next, a series of destructive adsorbents was compared; Fig. 10 summarizes these findings. Plotted are microliters, where 2 μL was injected every 6 min, vs moles of DMMP eluted. In this study 0.05 g of MgO samples was used (1.25×10^{-3} mol) and 70 μL of DMMP in total was injected (about 4.9×10^{-4} mol). Since two MgO moieties were necessary to destroy one DMMP molecule, or 6.2×10^{-4} $(MgO)_2$ equivalents, 70 μL is nearly the molar equivalent.

Note the remarkable result illustrated in Fig. 10. The $[Fe_2O_3]$AP-MgO was vastly superior to the lower surface area CP-MgO as well as $[Fe_2O_3]$CP-MgO, and significantly better than AP-MgO without Fe_2O_3 as a shell material. Clearly, Fe_2O_3 is very beneficial in this process of DMMP destructive adsorption, to the point that essentially a stoichiometric (not just surface) reaction took place. Thus, the Fe_2O_3 serves in some way to aid in exposing the inner reaches of the tiny MgO nanocrystals in a manner similar to the effect of Fe_2O_3 and other transition metal M_xO_y shell materials in chlorocarbon destructive adsorption.

The solid materials were analyzed by XRD before and after reaction. Before DMMP reaction, all the samples showed only reflections for MgO crystallites; no Fe_2O_3 was detected. After reaction, peaks due to $Mg_3(PO_4)_2 \cdot 5H_2O$ plus some remaining MgO were observed, with intensities varying depending on the destructive adsorbent used.

In another experiment, after reaction the AP-MgO and $[Fe_2O_3]$AP-MgO were heated under oxygen gas at 500°C for 3 h, which resulted in the formation of crystallites of $Mg_3(PO_4)_2$. Most of the MgO was converted to the phosphate in the AP-MgO case, and essentially all in the $[Fe_2O_3]$AP-MgO case.

Table 5 summarizes data concerning a series of experiments employing destructive adsorbent samples preheat treated in different ways (under vacuum or in a flow of

TABLE 5

Properties and Reaction Efficiencies of Destructive Adsorbents for Dimethylmethylphosphonate

Sample	Surface areas (m^2/g)		XRD Crystallite size (nm)		Breakthrough number[b]	Mol DMMP decomposed/ mol MgO
	Before reaction	After reaction[a]	Before reaction	After reaction		
AP-MgO	312	67	5	7	30	0.41
$[Fe_2O_3]$AP-MgO	252	27	5	7	58	0.50
CP-MgO	177	53	8	—	10 (6)[d]	0.23 (0.22)[d]
$[Fe_2O_3]$CP-MgO	116	45	8	10	6 (8)	0.30 (0.30)
CP-MgO(O_2)[c]	59	44	6	9	12 (6)	0.26 (0.20)
$[Fe_2O_3]$CP-MgO(O_2)[c]	146	91	9	11	14 (8)	0.35 (0.26)

[a] With 0.05-g sample and 70 μL DMMP (close to a 1 : 1 mol ratio).
[b] Number of μL DMMP (2 μL each injection) before breakthrough the bed.
[c] Dehydrated under a flow of O_2 instead of under vacuum.
[d] Parenthetical numbers are for aged samples.

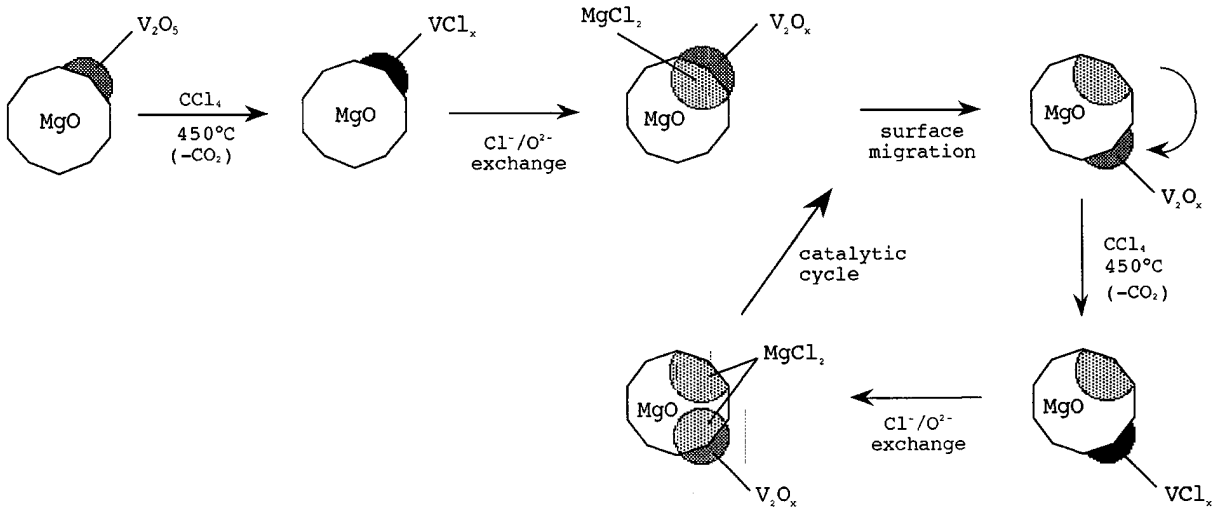

FIG. 11. Illustration of how V_2O_5 may catalyze Cl^-/O^{2-} exchange in CCl_4 destructive adsorption.

oxygen) and fresh vs aged samples. These data indicate that the dehydration step

$$Mg(OH)_2 \xrightarrow{500^\circ C} MgO + H_2O \qquad [7]$$

can be carried out under vacuum (best results) or under an O_2 flow (results still acceptable). Aging of samples for several weeks appeared to have a small detrimental effect on subsequent reactivity toward DMMP.

Also note that the $[Fe_2O_3]$AP-MgO sample reacted essentially quantitatively, considering that 2 mol MgO is necessary to destroy 1 mol of DMMP, so that the best moles of DMMP decomposed per mole of MgO ratios expected would be 0.50.

Sulfur Dioxide Adsorption on $[M_xO_y]$AP-CaO, where M = Fe

Results with $[Fe_2O_3]$AP-CaO and related systems have been reported earlier (2). A significant enhancement in SO_2 adsorption and conversion to a mixture of $CaSO_3/CaSO_4$/CaS at 500°C was realized.

DISCUSSION

The presence of small amounts of certain transition metal oxides has a remarkable catalytic effect on destructive adsorption processes in which the inner base oxide is consumed. The transition metals vanadium, manganese, and iron are particularly effective.

The key to understanding this rather unusual process may lie in the fact that the intermediate MX_n species ($X = O^{2-}$, Cl^-, SO_x^{n-}, PO_x^{n-}) may be mobile and that V, Mn, and Fe have available multiple oxidation states that allow rapid electron transfers during the catalytic process.

Considering the mobility concept further, Table 6 lists the melting points of some of the possible intermediate compounds. In particular, note the much lower melting points of the transition metal chlorides vs $MgCl_2$, $CaCl_2$, or the oxides. Therefore, at least for the chlorides it seems reasonable that the transition metal chloride would be formed

TABLE 6

Melting Points of Possible Intermediate Species (and Final Products) as an Indication of Mobility at a Reaction Temperature of 500°C

Compound	mp (°C)
VCl_3	d
VCl_4	−28
$MnCl_2$	650
$MnCl_3$	d
$FeCl_2$	670–674 subl.
$FeCl_3$	306 (d 315)
$Fe_2(SO_4)_3$	d 480
$CaCl_2$	782
$CaSO_4$	1450
CaO	2614
$MgCl_2$	714
$MgSO_4$	d 1124
MgO	2852
$Mg_3(PO_4)_2$	1184
V_2O_5	690
VO_2	1967
Mn_3O_4	1564
Mn_2O_3	1080 (loss of O)
MnO_2	535 (loss of O)
Fe_2O_3	1565
FeO	1369
Fe_3O_4	1594

Source. Handbook of Chemistry and Physics (D. R. Lide, Ed.), 75th ed., CRC Press, Boca Raton, FL, 1994–1995.

as an intermediate, and due to its mobility at reaction temperature could flow to defect or edge/corner sites on the MgO(CaO) nanocrystal (15). Next, exchange of Cl^- with O^{2-} could occur, and the sequence repeated, as illustrated in Fig. 11. Note that CCl_4 is proposed to attack the V_2O_5, producing VCl_x with CO_2 loss, the migration of VCl_x to corner sites of the MgO nanocrystal, where Cl^-/O^{2-} exchange takes, place regenerating the V_2O_5 (or VO_4). Then the sequence repeats itself (15).

Actually, the Cl^-/O^{2-} exchange step is not well understood. It seems likely that the availability of multiple oxidation states for the catalyst material would be beneficial; an illustration for the vanadium system is shown in Fig. 12. These illustrations are only intended to help in visualizing what may be happening. The individual steps are certainly not understood, nor is the initial Cl^-/O^{2-} exchange between CCl_4 and the transition metal oxide, although some attempts to illustrate this were reported recently for the CCl_4-CaO system (without the presence of a transition metal oxide) (4, 18).

A remarkable finding is that this type of catalysis was found to function in several cases, namely with chlorocarbon dehalogenation/oxidation, organophosphorus compound adsorption/decomposition, and sulfur dioxide adsorption/immobilization. It appears that this phenomenon may be fairly widespread (although recall that it did not occur with $CHCl{=}CCl_2$).

Due to this catalytic phenomenon, coupled with the high surface areas and reactive nature of nanoparticles in general, it is now possible to carry out essentially stoichiometric solid–gas reactions at moderate temperatures. This should open up new vistas in materials chemistry and catalysis.

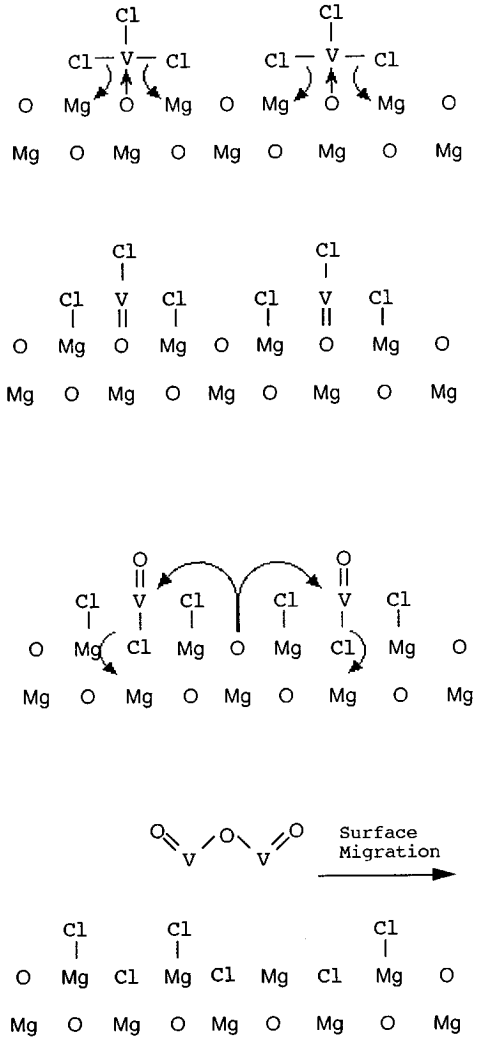

FIG. 12. Proposed process by which VCl_x exchanges Cl^-/O^{2-}.

ACKNOWLEDGMENTS

The support of the Army Research Office is acknowledged with gratitude. We also thank Professor P. M. A. Sherwood and Dr. Tiejun Wang for use of XPS equipment and help in obtaining spectra.

REFERENCES

1. Klabunde, K. J., Khaleel, A., and Park, D., *High Temperatures Material Sci.* **33**, 99 (1995).
2. Decker, S., and Klabunde, K. J., *J. Amer. Chem. Soc.* **118**, 12,465 (1996).
3. Klabunde, K. J., Stark, J., Koper, O., Mohs, C., Park, D. G., Decker, S., Jiang, Y., Lagadic, I., and Zhang, D., *J. Phys. Chem.* **100**, 12,142 (1996).
4. Decker, S., Lagadic, I., Klabunde, K. J., Michalowicz, A., and Moscovici, J., *Chem. Mater.* **10**, 674 (1998).
5. Jiang, Y., M. S. Thesis, Kansas State University, 1996.
6. (a) Li, Y. X., Koper, O. B., Atteya, M., and Klabunde, K. J., *Chem. Mater.* **4**, 323 (1992); (b) Klabunde, K. J., and Khaleel, A., U.S. Patent 5,712,219, January (1998); (c) Klabunde, K. J., and Khaleel, A., U.S. Patent 5,759,939, June (1998).
7. Sherwood, P. M. A., Photoelectron spectrometer computer operation and data analysis software reference manual, private communication.
8. Sherwood, P. M. A., "Practical Surface Analysis. Vol. 1. Auger and X-Ray Photoelectron Spectroscopy" (D. Briggs and M. P. Seah, Eds.), Appendix 3, Wiley, Chichester, 1990.
9. Scofield, J. H., *J. Electron Spec. Relat. Phenom.* **8**, 129 (1976).
10. Hutziner, O., Frei, R. W., Merian, E., and Pocchiari, F. (Eds.), "Chlorinated Dioxins and Related Compounds." Permagon, Oxford, 1982.
11. Exner, J. H., (Ed.), "Solving Hazardous Waste Problems: Learning from Dioxins." ACS Series 338, ACS, Washington, DC, 1987.
12. Thoma, H., *Chemosphere* **17**, 1369 (1988).
13. Yang, Y. C., Baker, J. A., and Ward, J. R., *Chem. Rev.* **92**, 1729 (1992).
14. Li, Y. X., and Klabunde, K. J., *Langmuir* **7**, 1388 (1991).
15. If these species are mobile, this would imply that some of the mobile species may be lost by migration from the catalyst/reactant bed. We have found that significant losses do not occur when the transition metal oxide loading is about 10% or less. However, in the case of high loadings, for example, 23% Fe_2O_3 on MgO, with the CCl_4 reaction some $FeCl_3$ left the bed and was converted downstream on the reaction walls to $FeCl_2$ plus Cl_2 (16, 17).
16. Mohs, C., Ph.D. thesis, Kansas State University, 1996.
17. Hooker, P. D., and Klabunde, K. J., *Env. Sci. Tech.* **28**, 1243 (1994).
18. Koper, O., Lagadic, I., and Klabunde, K. J., *Chem. Mater.* **9**, 838 (1997).